



Research Paper

The promoted effect of a metal-organic frameworks (ZIF-8) on Au/TiO₂ for CO oxidation at room temperature both in dark and under visible light irradiation



Yujuan Zhang^{a,b}, Qiuzhong Li^{a,b}, Chunxia Liu^{a,b}, Xinggang Shan^c, Xun Chen^a, Wenxin Dai^{a,b,*}, Xianzhi Fu^{a,**}

^a Research Institute of Photocatalysis, State Key Laboratory of Photocatalysis on Energy and Environment, Fuzhou University, Fuzhou 350002, China

^b Key Laboratory of Eco-Materials Advanced Technology (Fuzhou University), Fujian Province University, Fuzhou 350002, China

^c Zhejiang Harmony Photocatalytic Technology Co., Ltd, Shaoxing 312366, China

ARTICLE INFO

Keywords:

Metal-organic frameworks
TiO₂ supported Au catalyst
Electron transfer
Localized surface plasmon resonance of Au nanoparticles
Oxidation of carbon monoxide

ABSTRACT

A gold nanoparticle catalyst supported on the ZIF-8 (a metal-organic frameworks) modified TiO₂ (Au/ZIF-8-TiO₂) was prepared by self-assembly together with solvothermal and deposition-precipitation methods, which its performance of catalytic oxidizing CO was evaluated and compared with that of Au/TiO₂ and Au/ZIF-8, respectively. It was found that the incorporation of ZIF-8 into Au/TiO₂ could remarkably enhance the catalytic activity of Au/TiO₂ both in dark and under visible light irradiation. The characterization result of Au/ZIF-8-TiO₂ showed that the sheet of ZIF-8 was distributed on the surface of TiO₂ microspheres to enhance the surface roughness of TiO₂, which could effectively limit the migration and aggregation of Au nanoparticles (*i.e.*, enhancing the dispersion of Au nanoparticles at support) due to its large surface area and porosity. Moreover, Au/ZIF-8-TiO₂ owned a higher surface electron density of both Au nanoparticles and TiO₂ as compared to Au/TiO₂. It is proposed that ZIF-8 with abundant delocalized electrons of π bond could act as an electron donor for TiO₂ and Au in the structure of Au/ZIF-8-TiO₂, but it act as an electron transfer mediator to promote the electron transfer between Au and TiO₂ induced by the localized surface plasmon resonance of Au nanoparticles under visible light irradiation. These behaviors would promote the adsorption and activation of CO and O₂ at Au or TiO₂ sites, resulting in the enhanced CO oxidation.

1. Introduction

Catalytic oxidizing CO at low temperature has been exhibited the potentially commercial and industrial application in air purification, proton exchange membrane fuel cell, gas sensors and car exhaust systems [1–6]. Thereinto, the supported nano-gold catalysts on reducible oxide (*e.g.* TiO₂) have been arousing many researchers' attentions due to its highly efficient performance of catalytically oxidizing CO at low temperature [7,8]. Moreover, the catalytic activity of gold-based catalysts is considered to be susceptible to the size of Au nanoparticles, the nature of support and the interaction between Au and support [9–13] which contribute to increasing the surface electron densities of Au and promoting the adsorption and activation of CO and O₂. That is to say, enhancing the interaction (especially the electron transfer between Au nanoparticles and support) could improve the performance of Au/TiO₂ for oxidizing CO. Hereinto, we have ever introduced the visible light

into the reaction system of CO oxidation over Au/TiO₂, and found the promoted CO oxidation due to the increase in Au surface electron density induced by the localized surface plasmon resonance (LSPR) of Au nanoparticles [14].

It has been reported that the Au nanoparticles supported on zeolites, mesoporous materials, and activated carbons (AC) could be effectively controlled the size of Au particles and the distribution of Au particles [15–19] due to the supports' large surface area and the porosity. Moreover, some electron promoters, such as, C₃N₄, PANI and graphene [20–23], due to donate electrons into Au nanoparticles, was also contributive to the adsorption and activation of CO and O₂ at Au surface. The metal-organic frameworks (MOFs) are usually acted as CO₂ capturer thanks to their high surface area, huge porosity, tunable pore size and other functionalities [24,25]. Thereinto, ZIF-8 (Zn(MeIM)₂, MeIM: 2-methylimidazole) [26,27] as a representative material of MOFs possess an intersecting three-dimensional structural feature, highly thermal

* Corresponding author at: Research Institute of Photocatalysis, State Key Laboratory of Photocatalysis on Energy and Environment, Fuzhou University, Fuzhou 350002, China.

** Corresponding author.

E-mail addresses: daiwenxin@fzu.edu.cn (W. Dai), xzfu@fzu.edu.cn (X. Fu).

robust (over 400 °C), large pore size (diameter of 11.6 Å) and large surface area (BET, 1413 m²/g). Based on those properties, ZIF-8 had ever been introduced into the Au/TiO₂ to limit the migration and aggregation of Au nanoparticles, with the expectation of the higher dispersed Au nanoparticles and the smaller Au nanoparticles size [28–31]. It was believed that the narrower size distribution of Au nanoparticles would contribute to strengthening the LSPR of Au nanoparticles and reinforcing the interaction between Au and support. Moreover, since the ligand of ZIF-8 is 2-methylimidazole which owns abundant delocalized electrons of π bond [26], ZIF-8 may serve as an electron donor to provide electrons to TiO₂ and Au nanoparticles. Furthermore, the ZIF-8 could effectively decorate the optical properties of the support due to its strong light absorption at ultraviolet region [32]. In fact, MOFs and their derivatives have been considered as a kind of photocatalytic material (or support) for wastewater purification [33–35] and hydrogen production [36,37] due to the above semiconducting properties.

In this work we introduced ZIF-8 into the Au/TiO₂ catalyst for oxidizing CO under visible light irradiation or in dark. It is expected that ZIF-8 not only improve the dispersion of Au nanoparticles on TiO₂ support, but also act as an electron donor to supply electrons to Au nanoparticles and TiO₂ support by the interaction among Au, ZIF-8 and TiO₂. Moreover, it is also expected that the strong optical properties of ZIF-8 could improve the photo response of the samples. As was expected, the above advantages would be beneficial to the adsorption and activation of CO and O₂, and then promoting the oxidation of CO.

2. Experimental section

2.1. Preparation of catalysts

2.1.1. ZIF-8 (Zn(MeIM)₂, MeIM: 2-methylimidazole)

All chemicals were of analytical grade and used without further purification. ZIF-8 were prepared as follows: Firstly, 1.66 g of Zn (NO₃)₂·6H₂O (5.94 × 10⁻³ mol) was dissolved in 60.5 mL (1.49 mol) of methanol, and simultaneously, a 2-methylimidazole solution was prepared by mixing 9.75 g (0.12 mol) of 2-methylimidazole with 60.5 mL (1.49 mol) of methanol. Then, zinc nitrate solution was dropwisely added into the 2-methylimidazole solution under vigorous stirring with a magnetic stirrer at room temperature for 4 h. The final solution had a molar ratio of 1 (Zn(NO₃)₂·6H₂O): 20 (2-methylimidazole): 500 (methanol). Finally, this solution was centrifugated at 5000 rpm, and wash thoroughly with methanol. This procedure was repeated several times. The resultant precipitate were dried overnight at 80 °C [31,32].

2.1.2. TiO₂ and ZIF-8-TiO₂

Synthesis of mesoporous TiO₂ microspheres, 0.006 mol of NaOH was dissolved into 40 mL of pure ethanol, and then 2 mL of titanium trichloride solution was slowly added into the above solution under vigorous stirring with a magnetic stirrer. After reaction 30 min, the mixed solution was transferred to a 50 mL Teflon-lined autoclave and heated at 150 °C for 18 h. Finally, the precipitate collected through centrifugation at 8000 rpm, and rinsed by deionized water and pure ethanol for several times, then the product was dried overnight at 80 °C [38].

For the preparation of ZIF-8-TiO₂, the procedure was as the same to the synthesis of TiO₂, except that the different contents of ZIF-8 (1 wt%, 3 wt%, 4 wt%, 5 wt%) were added into the precursor of TiO₂, and after solvothermal, we also collected the final product by centrifugation with pure ethanol and deionized water, then dried overnight at 80 °C.

2.1.3. Au/TiO₂, Au/ZIF-8-TiO₂ and Au/ZIF-8

The catalysts of Au/TiO₂, Au/ZIF-8-TiO₂ and Au/ZIF-8 were prepared by deposition-precipitation method. Primarily, the 1.0 g support of TiO₂, ZIF-8-TiO₂ and ZIF-8 were homogeneously dispersed into the

100 mL distilled water. Secondly, 2.0 mL 0.01 g/mL HAuCl₄·3H₂O solution was added into the above suspension solution respectively, under vigorous stirring with a magnetic stirrer at room temperature for 1 h. Then, the 0.1 mol/L NaOH solution was used to adjust the pH value of the above solution until 10 and was subsequently reduced with the 0.1 mol/L alkalescent NaBH₄ solution. The precipitation was centrifuged and washed with deionized water for several times and dried at 80 °C overnight. The loading amount of Au for all samples was about 1.0 wt %.

2.2. Characterization of catalysts

X-ray diffraction (XRD) pattern was recorded on a BrukerD8 Advance powder X-ray diffractometer using Cu K α radiation ($\lambda = 0.15418$ nm) operated at 40 kV and 40 mA. Scanning electron microscopy (SEM) investigations were carried out on an FEI Nova NanoSEM 230 field-emission scanning electron microscope. Transmission electron microscopy (TEM) investigation together with an electron-diffraction image was carried out on a JEOL JEM-2010 EX with field emission gun at 200 kV. Energy dispersive X-ray (EDX) spectrum was also obtained with an EDX spectrometer (USA, EDax instrument). The optical properties of the samples were characterized by a Cary 500 UV-vis diffuse reflectance spectroscopy (DRS) with BaSO₄ as the internal reflectance standard. XPS was performed at a Quantum2000 system. XPS data were collected using the Al K α X-ray beam (1486.6 eV) operated on a Thermo Scientific ESCALab250 spectrometer. The C1s signal of 284.6 eV was used for the calibration of XPS data. The photocurrent was carried out by using three electrode cells. The resultant electrodes included the catalysts were served as the working electrode, with a platinum wire as the counter electrode and an Ag/AgCl (saturated KCl solution) electrode as the reference electrode.

2.3. Chemisorption of CO on catalysts

Fourier transform infrared (FT-IR) spectra instrument (Nicolet Nexus, Model 670) was measured at containing a controlled environmental quartz chamber equipped with two CaF₂ windows [20]. The adsorptions of CO on samples were measured with a Fourier transform infrared (FT-IR) spectra instrument (Nicolet Nexus, Model 670) containing a controlled environmental quartz chamber equipped with two CaF₂ windows. A self-supporting sample pellet (20 mg) of catalyst was mounted on a holder in the chamber. This sample was pretreated in a vacuum at a pressure of 10–1 Pa at 200 °C for 2 h. After cooling to room temperature, the gas was introduced into the sample (the amount of gas was enough to get a saturated adsorption at the surface of sample). 15 min later, an absorption spectrum was obtained. All spectra were recorded by a DTGS KBr detector in the transmission mode. For testing FT-IR under visible light irradiation, the visible light (490–760 nm) was introduced into the surface of sample thorough quartz chamber during the process of adsorbing gas.

Temperature programmed desorption (TPD) of samples were carried out with a Micromeritics Autochem2910 instrument [20]. Prior to the introduction of CO, the powder sample (50 mg) was firstly degassed in a high-purity He stream (20 mL min⁻¹) at 200 °C for 60 min. After cooled down to room temperature, a specific process for the sample proceeded as follows: (1) Introducing the CO gas into the sample for 30 min at room temperature with a flow rate of 20 mL min⁻¹ in a stream of about 2.5 vol% CO–He. (2) Switching He stream for 30 min. (3) Heating to 600 °C in a He stream at a ramping rate of 10 °C min⁻¹, and recording of a signal of thermal conductivity detector (TCD). Meanwhile, the mass signals of *m/z* = 28, 44, 18 were recorded. For testing TPD under visible light irradiation, the visible light (490–760 nm) was introduced into the surface of sample during the process of adsorbing CO.

2.4. Electron paramagnetic resonance (EPR) measurement for O_2 species

Electron paramagnetic resonance (EPR) measurements were carried out on a Bruker model A300 spectrometer. Typically, the 5 mg sample was placed on the top of testing tube. During the testing process for visible light, the visible light (490–760 nm) was introduced into the quartz cell for 4 min. The settings for the EPR spectrometer were as follows: center field, 3525.00 G; microwave frequency, 9.84 GHz; power, 6.36 mW.

2.5. Catalytic performances

The CO oxidation reactions were conducted in a fixed-bed flow reactor under an atmospheric pressure [20]. 0.5 g of catalyst with a grain of 0.2–0.3 mm was packed in a square quartz cell with a cooling water system which controlling the temperature of the reaction at 25 °C. And the total flow rate of feed stream was 100 mL min⁻¹ containing 0.3 vol % CO, 0.3 vol% O₂ and a balance He (CO/O₂ system). During photocatalytic reaction process, the visible light (produced by a 300 W Xenon lamp with an IR (> 760 nm) cut filter and another filter cut off light shorter than 490 nm) was introduced into the surface of the quartz cell. For testing the activity of catalysts in dark, the quartz cell was enclosed with Al foils to shut down light irradiation. The outlet gas was analyzed by a gas chromatograph system equipped with a thermal conductivity detector (Agilent 7890D, TDX-01).

The CO conversion and CO TOF conversion were calculated as follows:

$$\text{CO Conversion (X}_{\text{CO}}, \%) = ([\text{CO}]_{\text{in}} - [\text{CO}]_{\text{out}})/[\text{CO}]_{\text{in}} \times 100\% \quad (1)$$

$$\text{Turnover frequency of CO conversion (TOF, h}^{-1} \text{g}^{-1}) = (\text{X}_{\text{CO}} \times \text{N}_{\text{CO}} \times \text{M}_{\text{Au}})/(\text{m}_{\text{c}} \times \text{m}_{\text{Au}}) \quad (2)$$

Where N_{CO} – referred to the mol gas flow rate (100 mL min⁻¹ × 60 min h⁻¹ × 0.3 vol % ÷ 22400 mL mol⁻¹ = 8.03 × 10⁻⁴ mol h⁻¹), M_{Au} – referred to the mol weight of Au (197.0 g mol⁻¹), m_c referred to the weight of catalyst (0.5 g), m_{Au} – referred to the mass of Au in the reactor bed (0.5 g × 1.0% = 0.005 g).

3. Results and discussion

3.1. Catalyst characterizations

3.1.1. Structural properties

As shown in Fig. 1(A), the XRD patterns of the as-synthesized TiO₂, Au/TiO₂, TiO₂-ZIF-8 and Au/ZIF-8-TiO₂ samples were almost same, indicating that the introduction of ZIF-8 into TiO₂ and the loading of Au on support don't change the crystal structure of TiO₂. And diffraction peaks at 2θ values of 25.3°, 37.8°, 48.0°, 53.9° and 62.7° can be well corresponded to the (1 0 1), (0 0 4), (2 0 0), (1 0 5) and (2 0 4)

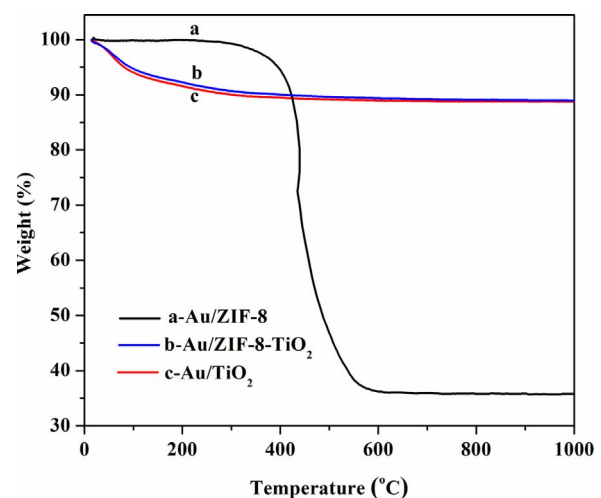
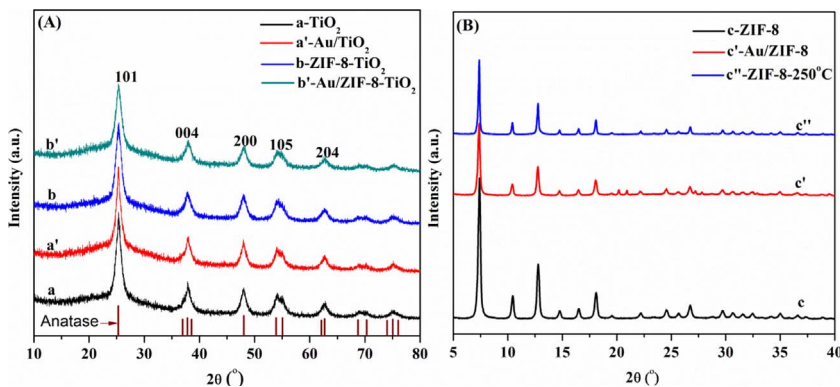


Fig. 2. Thermogravimetry pattern of (a) Au/ZIF-8, (b) Au/ZIF-8-TiO₂ and (c) Au/TiO₂ samples, respectively.

crystallographic planes of anatase TiO₂, respectively. Moreover, there were no the characteristic diffraction peaks of ZIF-8 and Au, indicating the lower contents or high dispersion of ZIF-8 and Au species distributed at the surface of the support. In addition, the XRD pattern in Fig. 1(B) shows that the loading of Au would not change the crystal structure of ZIF-8 (Au/ZIF-8 exhibited the same diffraction peaks as ZIF-8), indicating that Au nanoparticles could be highly dispersed at ZIF-8 surface. Besides, it is noted that the ZIF-8 sample which calcined at 250 °C didn't change the crystal structure of ZIF-8 (seen in Fig. 1(B)), indicating that ZIF-8 owned a highly thermal stability. This thermal robust could be also demonstrated by the TG results. As seen in Fig. 2, there was almost no weight loss over Au/ZIF-8 before 400 °C, which could guarantee the integrity of ZIF-8 in Au/ZIF-8-TiO₂. In fact, the introduction of ZIF-8 into Au/TiO₂ not only kept but even enhanced the thermal stability of Au/TiO₂ (curve b vs. curve c in Fig. 2).

3.1.2. Scanning electron microscopy and transmission electron microscopy

Fig. 3 shows the SEM and TEM images of Au/TiO₂, Au/ZIF-8-TiO₂ and Au/ZIF-8 samples. As seen in Fig. 3(a) and (b), both Au/TiO₂ and Au/ZIF-8-TiO₂ exhibited the similar microsphere morphology with the diameter of about 2 μm (attributed to the microsphere structure of TiO₂). However, the microsphere surface in Au/ZIF-8-TiO₂ was rougher than that in Au/TiO₂ (also observed from the TEM images of Fig. 3a' and b'), which may be caused by the lamellar ZIF-8 grown on the surface of TiO₂ microspheres. Moreover, the Au/ZIF-8-TiO₂ exhibited the narrower Au nanoparticles size than Au/TiO₂ (seen in Fig. 3a' and b'). It suggests that the introduction of ZIF-8 would be beneficial to control the size of Au nanoparticles [30]. In fact, Au/ZIF-8 sample exhibited a sheet of hexagon with the size at about 100 nm (seeing the

Fig. 1. (A) XRD patterns of (a) TiO₂, (a') Au/TiO₂, (b) ZIF-8-TiO₂ and (b') Au/ZIF-8-TiO₂; (B) XRD patterns of (c) ZIF-8, (c') Au/ZIF-8 and (c'') ZIF-8 treated at 250 °C.

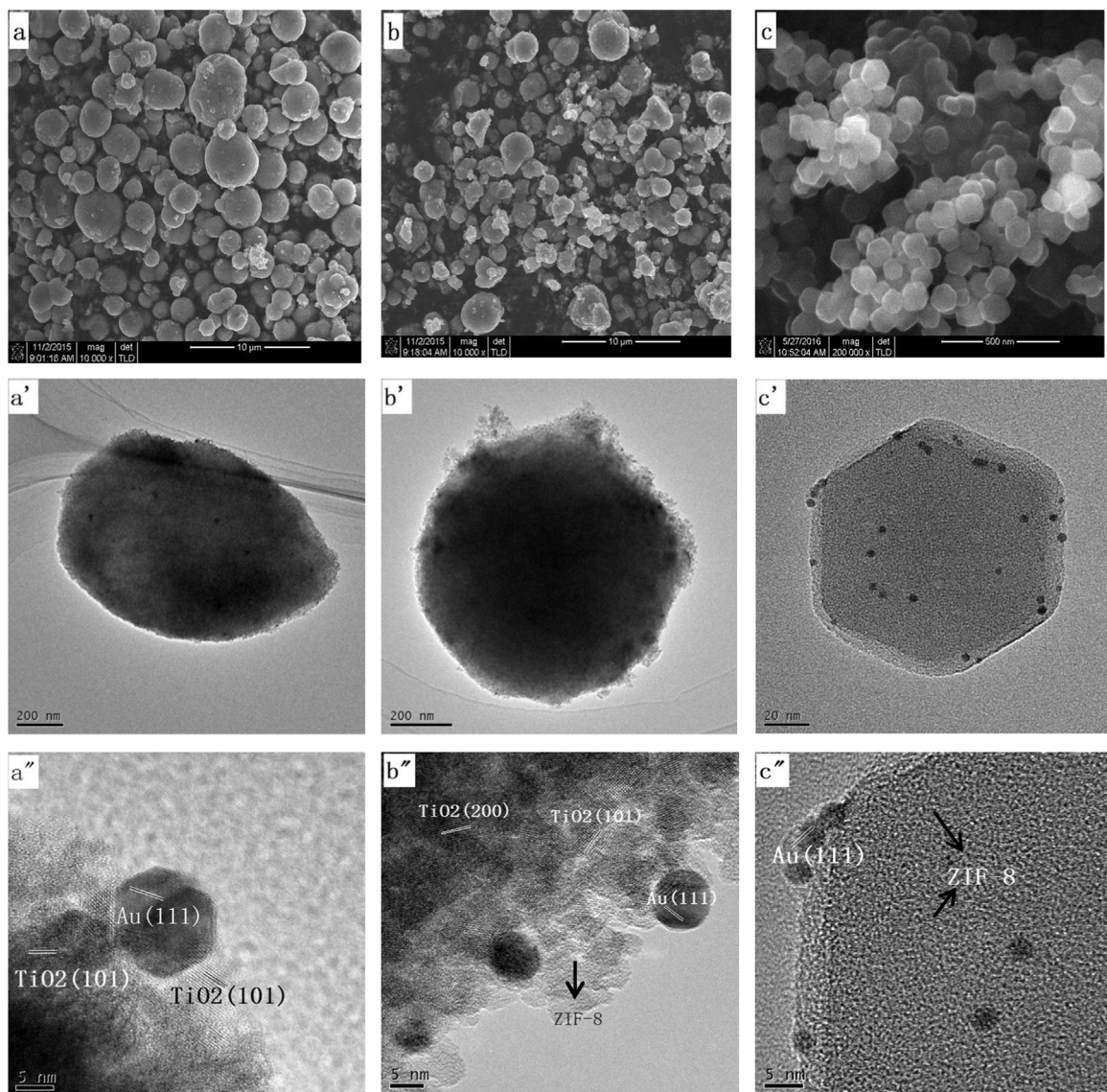


Fig. 3. SEM images of (a) Au/TiO₂, (b) Au/ZIF-8-TiO₂ and (c) Au/ZIF-8; TEM images of (a', a'') Au/TiO₂, (b', b'') Au/ZIF-8-TiO₂ and (c', c'') Au/ZIF-8 samples.

SEM image in Fig. 3c) and a smaller Au nanoparticle size (seeing the TEM images in Fig. 3c' and c'') than that in TiO₂ and ZIF-8-TiO₂. This indicates that the pure ZIF-8 could benefit to the formation of a highly dispersed and small Au nanoparticles.

3.1.3. UV-vis diffuse reflectance spectra

Fig. 4 shows the UV-vis absorption spectra of different samples. It was observed that TiO₂, ZIF-8-TiO₂, Au/TiO₂ and Au/ZIF-8-TiO₂ presented a TiO₂ intrinsic absorption peak at about 380 nm. While ZIF-8 and Au/ZIF-8 show a ZIF-8 intrinsic absorption peak at about 220 nm [39]. When compared to the support samples of TiO₂, ZIF-8-TiO₂ and ZIF-8, the Au/TiO₂, Au/ZIF-8-TiO₂ and Au/ZIF-8 samples with loading Au, exhibited an extra absorption peak at the visible region (about 540 nm), which can be attributed to the localized surface plasmon resonance (LSPR) of Au nanoparticles [40,41]. However, the peak intensity of the LSPR peak over Au/TiO₂ or Au/ZIF-8-TiO₂ was much stronger than that over Au/ZIF-8. Moreover, it is observed that Au/ZIF-8-TiO₂ exhibited a stronger LSPR peak with a red shift of the band as compared to Au/TiO₂. It suggests that the increase of the electron density on the surface of Au nanoparticles would lead to enhancement of their plasmonic absorption [42,43]. As for the red shift, a possible explanation is that the introduction of ZIF-8 changed the dielectric

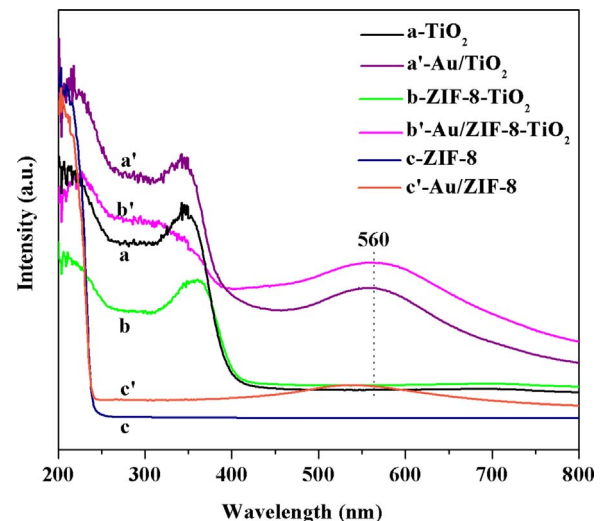
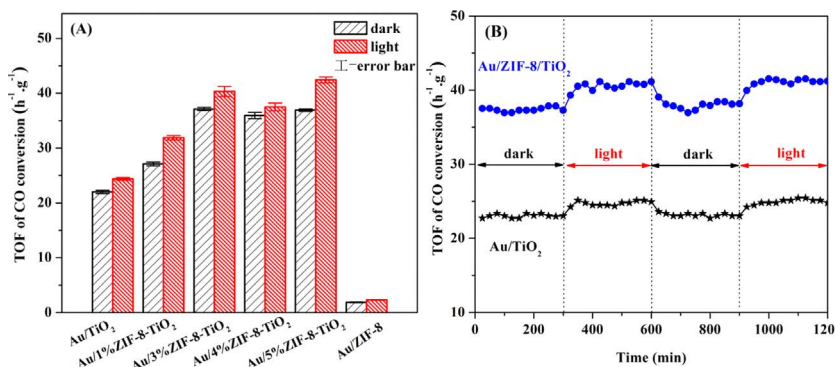


Fig. 4. UV-vis diffuse reflectance spectra of (a) TiO₂, (a') Au/TiO₂, (b) ZIF-8-TiO₂, (b') Au/ZIF-8-TiO₂, (c) ZIF-8, and (c') Au/ZIF-8 samples.



constant of TiO_2 support because the plasmonic absorption position of Au is highly dependent on the dielectric constant of the support [42,44]. In addition, Au/ZIF-8-TiO₂ and ZIF-8-TiO₂ also exhibited a red shift in the absorption edge of TiO_2 as compared to Au/TiO₂ and TiO₂, respectively. This may be attributed to the formation of N-Ti-O bond (seeing the following XPS results).

3.2. Catalytic performances

Fig. 5(A) shows the catalytic performances of Au/TiO₂, Au/ZIF-8-TiO₂ and Au/ZIF-8 samples toward the oxidation of CO. It is observed that the introduction of ZIF-8 into Au/TiO₂ could obviously enhance the conversion of CO. With the increase in ZIF-8 content, the CO conversion increased, but reached the optimal with the ZIF-8 content at 3.0 wt%. However, when the content of ZIF-8 was further increased, the CO catalytic performance approximately remained stable. Furthermore, with the introduction of the visible light into the reaction system, the CO conversions were obviously improved, and the Au/ZIF-8-TiO₂ exhibited the stronger light-driven effect than Au/TiO₂. Moreover, it is observed that Au/TiO₂ and Au/ZIF-8-TiO₂ (3.0 wt% ZIF-8) exhibited relatively stable catalytic activity both in dark and under visible light irradiation (see Fig. 5(B)). However, the Au/ZIF-8 sample did not exhibit apparently catalytic activity for oxidizing CO (the result not shown here), although it owned a much smaller size of Au nanoparticles than Au/TiO₂ or Au/ZIF-8-TiO₂. It could be deduced that the oxidation of CO on Au nanoparticles would also be related to the surface hydroxyls or surface oxygen species of TiO_2 to some extent [45,46].

3.3. Electron transfer on catalysts

3.3.1. X-ray photoelectron spectroscopy

As well known, the Au surface electron density plays an important role on the CO oxidation [13]. To compare the surface electron density of Au nanoparticles over Au/ZIF-8-TiO₂ with that of Au/TiO₂, the Au4f high-resolution XPS analyses of two samples after different reaction conditions were performed (the lower binding energy (BE) value of Au4f means the higher surface electron density of Au nanoparticles). As shown in Fig. 6(A), the BE values of Au4f7/2 and Au4f5/2 over both the fresh Au/ZIF-8-TiO₂ and Au/TiO₂ samples were lower than the standard BE of Au4f7/2 at 83.80 eV and Au4f5/2 at 87.50 eV for metallic Au sample [23], respectively. This indicates that Au nanoparticles over two samples were completely reduced to the metallic state, but they owned the higher surface electron density than the standard metallic Au due to the strong Au-support interaction [3]. Moreover, Au/ZIF-8-TiO₂ showed a lower Au4f7/2 BE value than Au/TiO₂ (83.50 eV vs. 83.70 eV). It is indicated that the introduction of ZIF-8 could enrich the surface electron density of Au, which is in accordance with the rich-electron properties of ZIF-8 (ZIF-8 donating electrons into Au). In fact, the fresh Au/ZIF-8 sample even exhibited a lower BE value of Au4f7/2 (83.40 eV) even than Au/ZIF-8-TiO₂ in Fig. 6(A). After reacted in dark, each sample exhibited the roughly same BE values of Au4f as that of the

Fig. 5. (A) TOF of CO conversion under visible light irradiation or in dark over (a) Au/TiO₂, (b–e) Au/ZIF-8-TiO₂ with 1.0 wt%, 3.0 wt%, 4.0 wt% and 5.0 wt% contents of ZIF-8, respectively, and (f) Au/ZIF-8. (B) The stability of CO conversion over Au/3%ZIF-8-TiO₂ under visible light irradiation or in dark.

fresh sample, respectively. It demonstrates that the reaction process in dark didn't change the electron density of Au nanoparticles. However, each sample after reacted in light, exhibited a lower surface electron density of Au nanoparticles as compared to the fresh sample (a negative shift in BE of Au4f), which may be caused by the localized surface plasmon resonance (LSPR) effect of Au nanoparticles [14]. Moreover, as compared to the Au/ZIF-8 and Au/TiO₂ samples, the Au/ZIF-8-TiO₂ exhibited the lowest BE value of Au4f (82.95 eV), after reacted in light.

It is noted that the fresh Au/ZIF-8 sample owned a higher surface electron density of Au nanoparticles than the fresh Au/ZIF-8-TiO₂ or Au/TiO₂ sample, but it showed a lower catalytic activity of oxidizing CO in dark or in light (seeing Fig. 5(A)). This indicates that the surface electron density of Au nanoparticles was not the sole role to determine the CO oxidation over the supported Au nanoparticle catalyst.

Furthermore, the high-resolution XPS results of Ti2p over Au/TiO₂ and Au/ZIF-8-TiO₂ samples treated by different conditions were also compared. As compared with the standard TiO₂ sample (owning the BE values of Ti2p3/2 at 458.50 eV and Ti2p1/2 at 464.20 eV for Ti⁴⁺) [21], both the Au/TiO₂ and Au/ZIF-8-TiO₂ samples exhibited a higher BE value of Ti2p (seeing Fig. 6(B)), indicating that the electrons maybe transferred from TiO_2 to Au nanoparticles over two samples due to the higher work function of TiO_2 [14]. However, Au/ZIF-8-TiO₂ owned a lower BE value of Ti2p than Au/TiO₂, meaning that ZIF-8 could enrich the surface electron density of Ti atoms. As compared to the two fresh samples, the reacted in dark didn't change the BE of Ti2p. However, the two samples reacted in light exhibited a negative shift in the BE of Ti2p, which may be attributed to the LSPR of Au nanoparticles.

Moreover, the O1s XPS spectra of Au/TiO₂, Au/ZIF-8-TiO₂ and Au/ZIF-8 samples were also compared. As shown in Fig. 6(C), the fresh Au/TiO₂ sample appeared two peaks at 530.20 and 532.95 eV, which could be assigned to the lattice oxygen (O_L) and surface hydroxyl group of TiO_2 (O_H), respectively [21]. As compared to the fresh Au/TiO₂ sample, the two O1s BE values of O_L and O_H species over the fresh Au/ZIF-8-TiO₂ sample made a slight negative shift of 0.10 eV (from 530.20 to 530.10 eV) and 0.30 eV (from 532.95 to 532.65 eV), respectively. It indicates that the addition of ZIF-8 into Au/TiO₂ could increase the surface electron densities of O atoms in Au/ZIF-8-TiO₂. However, the fresh Au/ZIF-8 sample showed a different O1s spectrum from the two formers. Here, the O1s spectrum could be deconvoluted into two components, which the two BE values of 532.10 and 533.70 eV were corresponded to the surface hydroxyl group (O_H) and surface carbonyl group (O_C) [47] of ZIF-8, respectively (seeing Fig. 6(D)). These O_C species may be caused by the probable adsorption of CO₂ [48].

It is noted that the peak intensity of O_H for the three reacted samples in dark suffered a fatal reduction as compared to that of the corresponding fresh sample. It suggests that some surface hydroxyl groups over the catalyst samples would be consumed during the reaction process in dark. However, the O1s BE value of O_H in each reacted sample almost remained the same as that of the fresh sample, indicating that the surface electron densities of surface oxygen species were not changed during the reaction process in dark. Nevertheless, the O1s BE

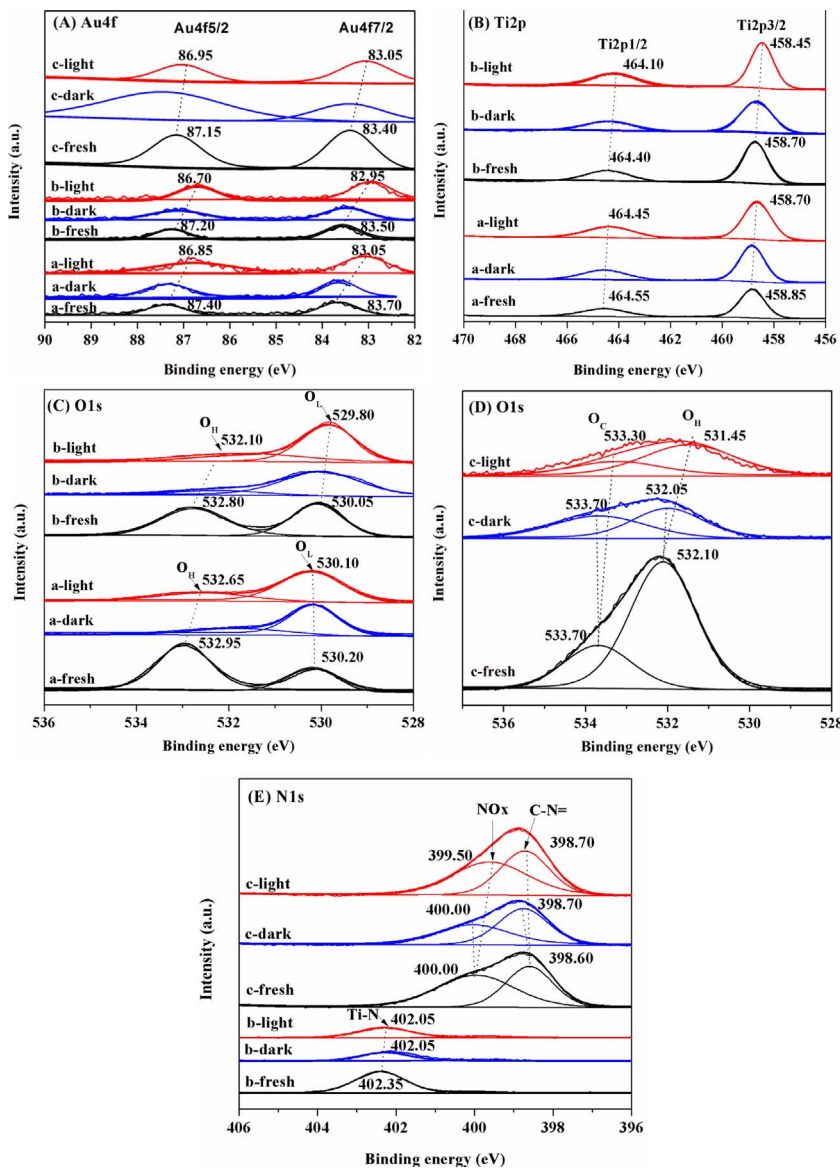


Fig. 6. High-resolution XPS spectra of Au4f (A), Ti2p (B), O1s (C, D) and N1s (E) over Au/TiO₂ (a), Au/ZIF-8-TiO₂ (b) and Au/ZIF-8 (c) samples under different treatment conditions, respectively. Here, curves of a-fresh (b-fresh or c-fresh), a-dark (b-dark or c-dark), and a-light (b-light or c-light) were referred to the fresh samples, the samples reacted in dark, and the samples reacted in visible light, respectively.

values of O_H for three samples reacted in visible light exhibited an obviously negative shift of 0.30 eV (Au/TiO₂), 0.70 eV (Au/ZIF-8-TiO₂) and 0.35 eV (Au/ZIF-8), respectively. It indicates that the visible light could promote the increase of the surface electron density of O atom in O_H species, and the promoted effect over Au/ZIF-8-TiO₂ was much stronger than that over Au/TiO₂ or Au/ZIF-8. Meanwhile, the O1s BE value of O_L for the reacted Au/ZIF-8-TiO₂ in light was lower than that of the fresh sample, but Au/TiO₂ remained the same O1s BE value of O_L after reacted in light. As can be seen, the introduction of ZIF-8 into Au/TiO₂ could effectively enrich the surface electron densities of oxygen species due to the interaction between ZIF-8 and Au/TiO₂. For the Au/ZIF-8 sample, the O1s BE value of O_C in ZIF-8 also remained the same after reacted in dark, but made a negative shift (from 533.70 to 533.30 eV) after reacted in visible light.

Fig. 6(E) shows the high resolution XPS spectra of N1s of Au/ZIF-8-TiO₂ and Au/ZIF-8. For the fresh Au/ZIF-8 sample, the peaks located at 398.60 and 400.00 eV could be attributed to the C–N bonds of ZIF-8 [49] and NO_x [50], respectively. For the fresh Au/ZIF-8-TiO₂ sample, only a strong N1s peak with the BE at 402.35 eV was observed, but the two peaks at 400.05 eV and 398.60 eV was not observed (the C–N structure covered). Here, the peak at 402.35 eV could be attributed to the formation of N–Ti–O structure [51]. As compared to the Ti–N

structure (with the typical N1s BE of 397.20 eV [50]), the N–Ti–O structure, formed by one nitrogen atom substituting the oxygen atom in the initial O–Ti–O structure, exhibited a high N1s BE value (*i.e.*, owned a lower electron density of N atoms). That is to say, the O atom adjacent to Ti atom in N–Ti–O structure would probably accept electrons from the N atom adjacent to Ti atom [52], resulting in the increase in surface electron density of the lattice oxygen in TiO₂ (also seeing Fig. 6C). Moreover, the reacted Au/ZIF-8-TiO₂ exhibited a lower N1s BE value of N–Ti–O structure than the fresh sample, indicating that the increase in surface electron density of N atom during the reaction process. However, the reacted Au/ZIF-8 exhibited a higher N1s BE value of C–N than the fresh sample, indicating that ZIF-8 donates electrons to Au nanoparticles over Au/ZIF-8 during the reaction process.

Based on the above XPS results, it is proposed that there existed a charge transfer behavior among Au nanoparticles, ZIF-8 and TiO₂ over Au/ZIF-8-TiO₂. Maybe due to its abundant delocalized electrons of π bond, the introduction of ZIF-8 into Au/TiO₂ could donate electrons to TiO₂ and Au, resulting in a higher surface electron density of Au and TiO₂ than that of Au/TiO₂. This electron transfer behavior between ZIF-8 and TiO₂ or Au could be described in Fig. 7. Moreover, the introduction of visible light could further enhance the surface electron densities of TiO₂ and Au over both Au/ZIF-8-TiO₂ and Au/TiO₂ due to

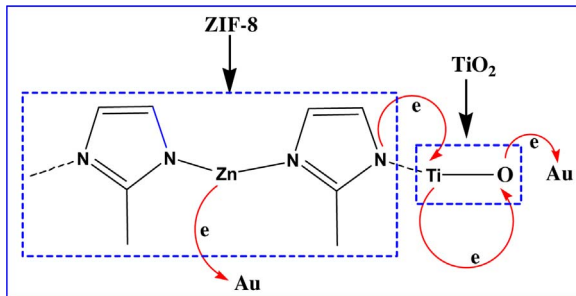


Fig. 7. The possible charge transfer behaviour among Au, TiO_2 and ZIF-8 during the process of forming Au/ZIF-8- TiO_2 structure. On the one hand, ZIF-8 (with abundant delocalized electrons of π bond) donates electrons to TiO_2 by N–Ti–O structure and then to Au nanoparticles; On the other hand, ZIF-8 also directly donates electrons to the adjacent Au nanoparticles.

the LSPR of Au nanoparticles, but the surface electron density of Au and TiO_2 over Au/ZIF-8- TiO_2 was higher than that over Au/ TiO_2 , respectively.

3.3.2. Photocurrent test

To further compare the electron transfer behavior occurred on Au/ZIF-8- TiO_2 with that on Au/ TiO_2 and Au/ZIF-8, especially under visible light irradiation, the photocurrent tests of three samples were performed. **Fig. 8** shows the transient photocurrent response of Au/ TiO_2 , Au/ZIF-8- TiO_2 and Au/ZIF-8 during the several on-off cycle of visible light. As compared to the respective initial state, the photocurrent intensity of Au/ TiO_2 and Au/ZIF-8- TiO_2 decreased with the increase in the on-off cycles of light, which could be attributed to the LSPR effect of Au nanoparticles and the electric charge rearrangement between Au nanoparticles and support [3]. However, the photocurrent of Au/ZIF-8- TiO_2 was stronger than that of Au/ TiO_2 , indicating that the ZIF-8 maybe act as an efficient charge mediator over Au/ZIF-8- TiO_2 under visible light irradiation. Note that the photocurrent intensity of Au/ZIF-8 was far lower than that of Au/ TiO_2 or Au/ZIF-8- TiO_2 , indicating that ZIF-8 itself is not a suitable support for transferring and separating electrons induced by the LSPR of Au nanoparticles in the absence of TiO_2 . This result shows that ZIF-8 maybe acted as an electron transfer mediator to improve electron transfer between Au and TiO_2 . A detailed explanation will be described in the Section of 3.7.

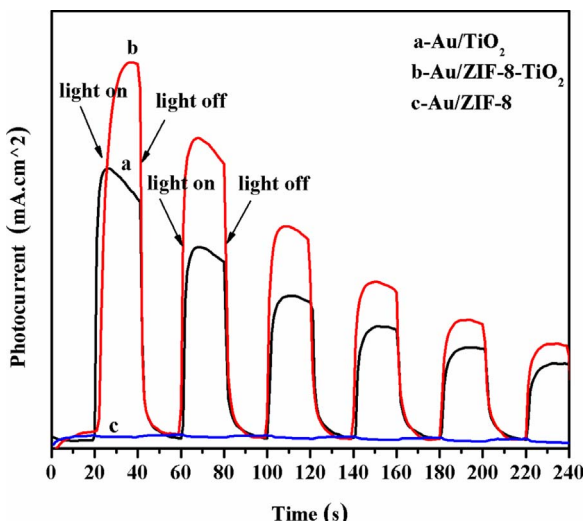


Fig. 8. Photocurrent spectra of (a) Au/ TiO_2 , (b) Au/ZIF-8- TiO_2 and (c) Au/ZIF-8 samples. Here, Au/ZIF-8 did not show any photocurrent under visible light irradiation.

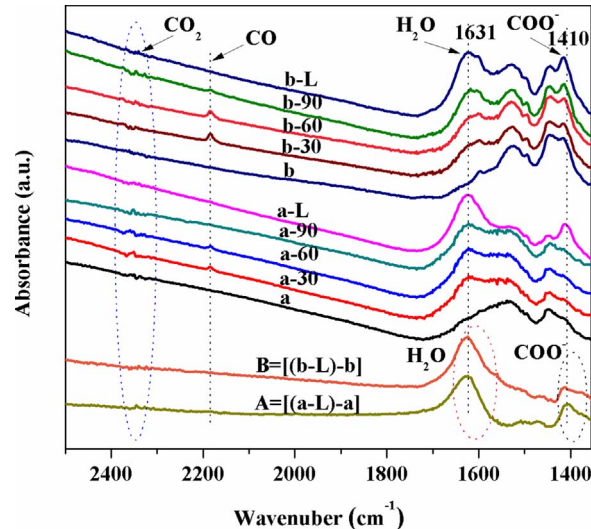


Fig. 9. FT-IR absorption spectra of adsorption CO on (a) Au/ TiO_2 and (b) Au/ZIF-8- TiO_2 samples. Curves of a (b), a-30 (b-30), a-60 (b-60), a-90 (b-90) and a-L (b-L) represented the spectra of Au/ TiO_2 (Au/ZIF-8- TiO_2) absorbing 0 min, 30 min, 60 min, 90 min and the treatment of visible light, respectively; Curve A or B represented the curve a or b subtracted from curve a-L or b-L, respectively.

3.4. FT-IR test for adsorbing CO

As well known, the increase in surface electron densities of both Au nanoparticles and TiO_2 support can benefit to the adsorption and activating of CO and O_2 [53], which further promote the oxidation of CO. To demonstrate it, the chemisorption behaviors of CO and O_2 over samples were performed.

Considering that the surface electron density of Au nanoparticles are intimately related to the adsorption and activation of CO at Au sites [54], the FT-IR testing were performed to investigate the adsorption properties of CO at Au/ TiO_2 , Au/ZIF-8- TiO_2 and Au/ZIF-8 samples. As shown in **Fig. 9**, after adsorbing CO for 30 min (curves of a-30 and b-30), both Au/ TiO_2 and Au/ZIF-8- TiO_2 exhibited a CO band at ca. 2185 cm^{-1} assigned to CO linearly bonded on sample [55,56]. After 60 min (curves of a-60 and b-60), both two samples experienced a slight increase in the CO peak, but Au/ZIF-8- TiO_2 showed a stronger CO adsorption than Au/ TiO_2 . However, the CO absorption peaks of Au/ TiO_2 was almost disappeared after 90 min (curve of a-90), but Au/ZIF-8- TiO_2 still remained some CO species (curve of b-90). This maybe because the CO adsorbed at Au sites could directly react with the surface hydroxyl group in the absence of O_2 [57]. However, Au/ TiO_2 could be favor of this reaction as compared to Au/ZIF-8- TiO_2 .

In fact, the process of CO oxidized by surface hydroxyls could be also demonstrated by the formation of H_2O and carboxyl group. As seen in **Fig. 9**, during the above process of adsorbing CO, two new peaks located at ca. 1631 and 1410 cm^{-1} (assigned as the bending vibration mode of H_2O and carboxyl group, respectively) appeared on Au/ TiO_2 and Au/ZIF-8- TiO_2 , which could be attributed to the H_2O and carboxide species (surface monodentate formate or carbonate-like species (the carbonyl stretching region of 1450 – 1350 cm^{-1} [58])) generated by CO reacting with surface hydroxyls [57]. With the introduction of visible light (curves of a-L and b-L), the CO peak on two samples disappeared with the concomitant increase of H_2O peak, indicating that visible light could promote the reaction of CO with surface hydroxyls in the absence of O_2 . Further comparing the changes of H_2O and carboxyl group over two samples during the process of adsorbing CO (curve A vs. curve B), it can be seen that both the formation amount of H_2O and carboxyl group over Au/ TiO_2 was more than that over Au/ZIF-8- TiO_2 , also indicating that Au/ TiO_2 was favor of the reaction of CO with surface hydroxyls in the absence of O_2 in dark or in light compared with Au/ZIF-8- TiO_2 . However, as for Au/ZIF-8, there was almost no change after adsorbing

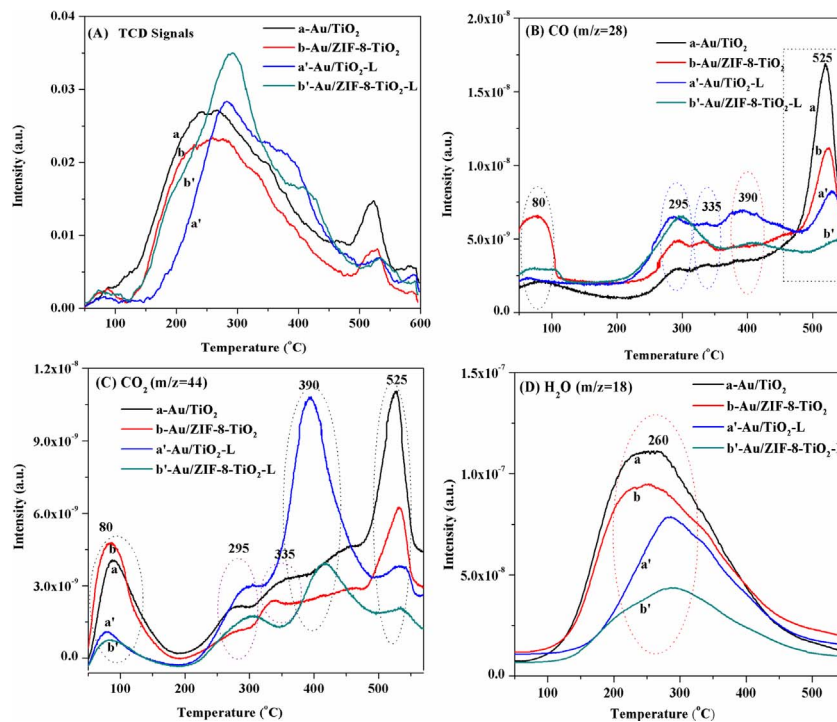


Fig. 10. TPD spectra of Au/TiO₂ and Au/ZIF-8-TiO₂ samples: (A) TCD signals, (B) CO Mass signals, (C) CO₂ Mass signals and (D) H₂O Mass signals. Curves of a and b represented the dark absorption of Au/TiO₂ and Au/ZIF-8-TiO₂, respectively; Curves of a' and b' represented the light absorption of Au/TiO₂ and Au/ZIF-8-TiO₂, respectively.

CO (seeing Fig. S1 in support information (SI)). Moreover, the CO adsorption could not cause the change in the peak located at 1631 cm⁻¹, indicating that CO did not react with the surface hydroxyls over Au/ZIF-8 in the absence of O₂.

Note that the CO₂ peak at 2335 cm⁻¹ appeared during the process of Au/TiO₂ adsorbing CO in dark, but it was not obvious over Au/ZIF-8-TiO₂ under the same process. This indicates that some CO may be oxidized into other species (not CO₂) by surface hydroxyls in the absence of O₂. Moreover, no CO₂ peak was observed over two samples with the introduction of visible light, it suggests that visible light maybe suppress the adsorption of CO₂ at two samples.

3.5. TPD test for adsorbing CO

The CO adsorption behaviors over Au/TiO₂ and Au/ZIF-8-TiO₂ can be also investigated by the temperature-programmed desorption (TPD) test. As seen in Fig. 10(A), Au/TiO₂ and Au/ZIF-8-TiO₂ showed different TCD signals during the TPD process after adsorbing CO in dark or in light. Furthermore, the Mass signal of CO showed that there were five desorption regions located at ca. 80, 295, 335, 390 and 525 °C over two samples in dark, respectively (seeing Fig. 10(B)), indicating that different adsorption states of CO existed at the sample surface after adsorbing CO in dark. However, these desorption peaks of Au/TiO₂ were different from those of Au/ZIF-8-TiO₂. It can be seen that the intensity of desorption peak at 80 °C over Au/ZIF-8-TiO₂ was evidently stronger than that over Au/TiO₂ in dark, indicating that Au/ZIF-8-TiO₂ could benefit to the adsorption of CO at a low temperature as compared to Au/TiO₂. Moreover, this desorption process of the adsorbed CO at 80 °C would cause CO₂ desorption at 80 °C (seeing Fig. 10(C)), indicating that this adsorbed CO species could be partly converted into CO₂ (i.e., CO reacting with surface hydroxyls [57]). However, Au/TiO₂ also exhibited a desorption peak of CO₂ at 80 °C which was stronger than that of Au/ZIF-8-TiO₂, meaning that this adsorbed CO species at the former could be more easily oxidized by surface hydroxyls into CO₂ in the absence of O₂ than that of the latter, consistent with the FT-IR result in Fig. 9. When adsorbing CO under visible light irradiation, the above desorbed peaks of CO and CO₂ at the low temperature over two samples suffered a fatal decrease, this maybe because the visible light could drive the

rapid conversion of the adsorbed CO to CO₂ which could be degassed during the adsorbing process. This also shows that the visible light could promote CO conversion into CO₂, in accordance with the analysis results of FT-IR in Fig. 9.

Moreover, the intensities of the two desorbed CO peak at ca. 295 and 335 °C over Au/ZIF-8-TiO₂ were also stronger than that over Au/TiO₂ after adsorbing CO in dark (seeing Fig. 10(B)). Moreover, the two corresponding CO₂ peaks at ca. 295 and 335 °C (seeing Fig. 10(C)) were also observed over two samples, but the intensities of two CO₂ peaks over Au/ZIF-8-TiO₂ were less than those over Au/TiO₂, respectively. This indicates that other adsorbed CO species (or the formed carboxyl species induced by the adsorbed CO reacting with surface hydroxyls [57]) could be also converted into CO₂, which more easily occurred on Au/TiO₂. Note that the process of CO converted into CO₂ at 295 and 335 °C would cause the desorption of H₂O at 260 °C (seeing Fig. 10(D)), further demonstrating that the adsorbed CO would react with the surface hydroxyls to form CO₂ and H₂O in the absence of O₂ (seeing Fig. 9). As compared to the CO adsorption in dark, the CO adsorption under visible light irradiation would cause the increase in the two desorption peaks of CO at 295 and 335 °C over Au/TiO₂, but only cause a stronger peak of CO desorption at 295 °C over Au/ZIF-8-TiO₂. Moreover, the two desorption peaks of CO₂ at 295 and 335 °C become one desorption peak of CO₂ at 295 °C over two samples when adsorbing CO under visible light irradiation, indicating that visible light maybe changed the adsorption state of CO and then its oxidation into CO₂ over two samples, especially over Au/ZIF-8-TiO₂. Since the above samples were pretreated at 200 °C prior to adsorbing CO, the above desorption peaks of CO, CO₂ and H₂O at 295 and 335 °C (above 200 °C) could be also partly originated from the decomposition of carboxide species remained at the sample surface. In addition, Au/TiO₂ exhibited a larger desorption peak of CO at ca. 525 °C than Au/ZIF-8-TiO₂ after adsorbing CO in dark. The corresponding desorption peak of CO₂ at 525 °C over Au/TiO₂ was also larger than that over Au/ZIF-8-TiO₂. These desorbed CO and CO₂ at a high temperature maybe resulted from the decomposition of other carboxide species (e.g., COO⁻) adsorbed at Au/TiO₂ and Au/ZIF-8-TiO₂ samples. These carboxide species could be formed by the adsorbed CO reacting with surface hydroxyls [57], but also originated from the remained species during the process of preparing catalyst samples (both

two samples exhibited the desorption peaks at this temperature in TCD signals even if no adsorbing CO in dark, (seeing Fig. S2 in SI). However, Au/TiO₂ owned a more carboxide species (exhibiting the stronger desorption peaks of CO and CO₂ at 525 °C) than Au/ZIF-8-TiO₂, also indicating that the former could be favor of the reaction of CO with surface hydroxyls in the absence of O₂. As compared to the above result of adsorbing CO in dark, the introduction of visible light into the process of adsorbing CO would cause the apparent decrease in the desorption peak of CO at 525 °C over both Au/TiO₂ and Au/ZIF-8-TiO₂ samples, but led to the great increase in a new desorption peak of CO at ca. 390 °C (seeing curves a' and b' in Fig. 10(B)). This indicates that the visible light may be beneficial to the activation of carboxide species over two samples, resulting in its decomposition at a lower temperature. The CO₂ mass signals in Fig. 10(B) also showed that the desorption peak of CO₂ over two samples increased apparently after visible light irradiation, and the desorption temperature was shifted from 525 °C to 390 °C.

Overall, the CO peak desorbed at low temperature (80 °C) over Au/ZIF-8-TiO₂ was larger than that over Au/TiO₂, while the CO peak desorbed at high temperature (525 °C) over the former was far less than that over the latter. This shows that Au/ZIF-8-TiO₂ could benefit to the adsorption of CO and its activation as compared to Au/TiO₂. However, considering that the process of oxidizing CO in Fig. 5(A–B) was proceed in the presence of O₂, the adsorption and activation of O₂ on catalyst samples may be also crucial [46].

3.6. Electron paramagnetic resonance (EPR) measurement for active oxygen species

It was reported that at room temperature, dioxygen was very difficult to dissociate into atomic oxygen, and instead molecular oxygen was usually activated in the form of O₂ species [59,60]. At less than or equal to room temperature, the presence of molecular oxygen derived superoxide and peroxide species exposed to the air atmosphere could even be directly identified by EPR spectra [60]. Fig. 11 shows the EPR spectra of Au/TiO₂ and Au/ZIF-8-TiO₂ at room temperature at air atmosphere. A signal located at $g = 1.9998$, ascribed to O₂[−] radicals [61,62], was observed over two samples. However, the signal of Au/ZIF-8-TiO₂ was stronger than Au/TiO₂, indicating that the former could benefit to the activation of O₂ as compared to the latter. Moreover, the signal of each sample under visible light irradiation was stronger than that in dark, indicating that visible light could promote the activation of O₂ [22,23,63]. As can be seen, the more O₂[−] radicals existed at Au/ZIF-8-TiO₂ could be advantageous to the oxidation of CO as compared to

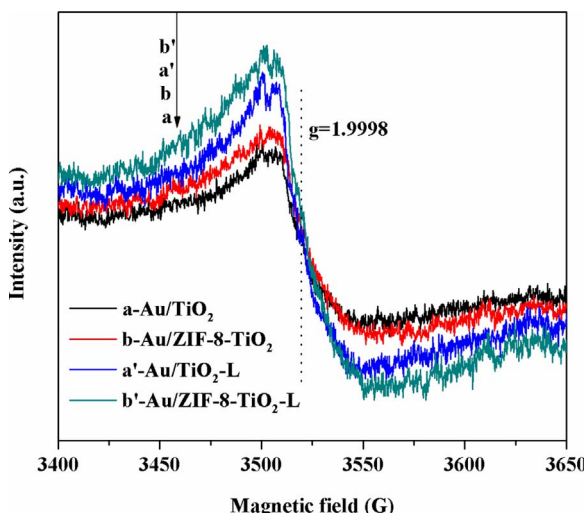


Fig. 11. The EPR spectra of (a) Au/TiO₂ in dark, (b) Au/ZIF-8-TiO₂ in dark, (a') Au/TiO₂ in visible light, and (b') Au/ZIF-8-TiO₂ in visible light.

Table 1

The correlation among Au surface electron density, CO (O₂) adsorption and CO conversion over Au/TiO₂ and Au/ZIF-8-TiO₂.

samples	Surface electron density of Au and TiO ₂	CO adsorption	O ₂ adsorption	CO conversion
Au/TiO ₂	Lower	Weak	Weaker	Lower
Au/ZIF-8-TiO ₂	Higher	Stronger	Stronger	Higher

Au/ZIF-8-TiO₂. Note that no EPR signal was observed over Au/ZIF-8 in dark or in visible light (seeing Fig. S3 in SI), indicating that the pure ZIF-8 could not activate the adsorbed O₂. This may be one reason that Au/ZIF-8 could not catalytically oxidize CO in dark or under visible light irradiation.

3.7. Proposed mechanism of CO oxidation over Au/ZIF-8-TiO₂

Based on the above results, it could be concluded that the catalytic oxidation CO over Au/TiO₂ and Au/ZIF-8-TiO₂ was closely related to the surface electron densities of Au species and support, which was vital to the adsorption and activation of CO and O₂. As compared to Au/TiO₂, Au/ZIF-8-TiO₂ showed the lower BE value of Au4f and Ti2p and O1s (i.e., a higher electron density of Au and TiO₂ surface). The higher electron density on sample surface is inclined to form activated species of reaction, and then it would show a stronger adsorption and activation of both CO and O₂, which would contribute to the higher CO conversion. These correlations could be concluded in Table 1.

During the reaction process in dark, the increase in surface electron densities of both Au and TiO₂ sites could be attributed to the donating electron behavior of ZIF-8 due to its abundant delocalized electrons of π bond. This behavior should be completed during the process of preparing Au/ZIF-8-TiO₂.

As for the reaction process of oxidizing CO over Au/ZIF-8-TiO₂ under visible light irradiation, since ZIF-8 itself could not be excited by visible light (seeing DRS spectrum in Fig. 4), it seems not to donate electrons to TiO₂ and Au according to the explanation for electron transfer among ZIF-8, TiO₂ and Au in Fig. 7. How did ZIF-8 promote the electron transfer (Au/ZIF-8-TiO₂ exhibiting a larger photocurrent than Au/TiO₂ in Fig. 8) and enhance the surface electron density of Au and TiO₂ (seeing the XPS result in Fig. 6)?

In fact, Wen et al. [36,37,42] have reported that functionalized MOFs could act as electron transfer mediator to facilitate the charge transfer of photo-generated electrons between active sites and then the formation of active species. Here, the functionalized MOFs with a semiconducting property could be light-excited during the reaction process. However, for the Au/ZIF-8-TiO₂ sample in this work, only Au nanoparticles could be light-excited by its LSPR under visible light irradiation, the insulator ZIF-8 (not excited by visible light due to its higher level of LUMO) was very difficult to accept the photo-generated electrons from Au nanoparticles. The unobserved photocurrent for Au/ZIF-8 sample in Fig. 8 also seemed to confirm it. As can be seen, there may exist other approaches to complete the electron transfer process.

In our previous work [20], it suggested that the photo-generated electrons induced by the LSPR of Au nanoparticles could transfer reversely to TiO₂ support, although the Femi level of TiO₂ is higher than that of Au. This because the excited state of Au nanoparticles induced by LSPR owns a little higher level than the conducting band level of TiO₂. The observed photocurrent for Au/TiO₂ sample in Fig. 8 also confirmed this inference. Considering that the photocurrent value of Au/ZIF-8-TiO₂ is higher than that of Au/TiO₂ in Fig. 8, it can be supposed that there maybe exists another new approach to accept the photo-generated electrons from Au nanoparticles.

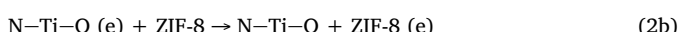
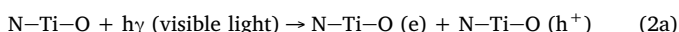
Based on the XPS results in Fig. 6, we think that ZIF-8 can offer electrons to TiO₂ by forming N–Ti–O structure and then to Au

nanoparticles (seeing Fig. 7). However, this formed N–Ti–O structure may be excited by the visible light, which can be confirmed by the broader light absorption region of Au/ZIF-8-TiO₂ and ZIF-8-TiO₂ as compared to Au/TiO₂ and TiO₂, respectively (seeing Fig. 4). With the viewpoint of reverse electron transfer from Au to TiO₂ over Au/TiO₂ induced by LSPR effect of Au nanoparticles [20], we think that some new reverse electron transfer processes may also occur on Au/ZIF-8-TiO₂ under visible light irradiation. A proposed process can be described as follows:

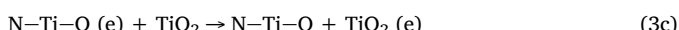
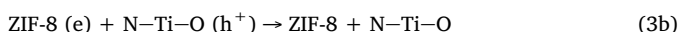
I A reverse electron transfer from Au to TiO₂ adjacent to N–Ti–O:



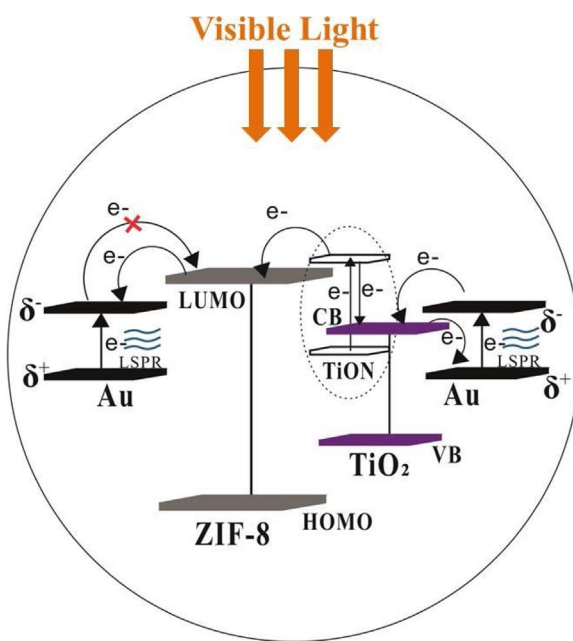
• A reverse electron transfer from N–Ti–O to ZIF-8:



• The forward electron transfer from ZIF-8 to Au, ZIF-8 to N–Ti–O, N–Ti–O to TiO₂, and TiO₂ to Au, respectively:



During the above process, the light-excitation of N–Ti–O structure could make ZIF-8 act as an electron transfer mediator to enhance the surface electron density of Au nanoparticles and TiO₂. It is noted that the N–Ti–O structure is closely adjacent to O–Ti–O (TiO₂), the photo-generated electrons from N–Ti–O are mainly transferred to Au by TiO₂. This proposed process could also be described as **Scheme 1**.



Scheme 1. Proposed schematic of electron transfer among Au, TiO₂ and ZIF-8 sites over Au/ZIF-8-TiO₂ under visible light irradiation. Here, the light-excitation of N–Ti–O structure could make ZIF-8 act as an electron transfer mediator to enhance the surface electron density of Au nanoparticles and TiO₂.

As compared to Au/TiO₂, Au/ZIF-8-TiO₂ owned a higher surface electron density of both Au and TiO₂ due to the electron transfer between ZIF-8 and Au or TiO₂, which resulted in the enhanced adsorption and activation of CO and O₂, and then the higher catalytic activity of oxidizing CO in the presence of O₂ under visible light irradiation.

4. Conclusions

In this work, the Au/ZIF-8-TiO₂ samples were prepared by in-situ self-assembly and deposition-precipitation methods. After comparing its performance of oxidizing CO with that of Au/TiO₂, the following conclusions can be drawn:

- (I) Au/ZIF-8-TiO₂ showed a better performance toward CO oxidation than Au/TiO₂ at room temperature in dark or under visible light irradiation.
- (II) The XPS results showed that Au/ZIF-8-TiO₂ exhibited the higher surface electron density of both Au and TiO₂ than Au/TiO₂, which could be attributed to the electron transfer between ZIF-8 and TiO₂ or Au nanoparticles. Moreover, Au/ZIF-8-TiO₂ was more sensitive to visible light than Au/TiO₂ due to the formation of N–Ti–O structure, resulting in the higher electron density of Au nanoparticles and TiO₂ induced by the LSPR effect of Au nanoparticles. This promoted electron transfer behavior induced by visible light could be demonstrated by a photocurrent test.
- (III) The results of FI-IR, TPD-mass and EPR showed that Au/ZIF-8-TiO₂ could benefit to the adsorption of both CO and O₂ and their activation as compared to Au/TiO₂, e.g., TPD results showed that a larger CO desorbed peak at low temperature occurred on Au/ZIF-8-TiO₂, but a larger CO desorbed peak at high temperature over Au/TiO₂. However, the adsorbed CO on Au/TiO₂ could be more easily reacted with the surface hydroxyls than that on Au/ZIF-8-TiO₂ in the absence of O₂.
- (IV) TEM images showed that the introduction of ZIF-8 into Au/TiO₂ could limit the aggregation of Au nanoparticles. However, Au/ZIF-8, with a much smaller size of Au nanoparticles than Au/ZIF-8-TiO₂ or Au/TiO₂, could not catalytically oxidize CO in the presence of O₂ both in dark and under visible light irradiation, which may be attributed to the suppressed adsorption and activation of O₂ on Au/ZIF-8.

Overall, it was suggested that ZIF-8 (as one kind of MOFs) probably acts as an electron donor (the constituted 2-methylimidazole ligand owning abundant delocalized electrons of π bond) to enrich the surface electron densities of both Au and TiO₂, resulting in the adsorption and activation of CO and O₂, and then promoting the CO oxidation over Au/ZIF-8-TiO₂. Moreover, ZIF-8 can act as electron transfer mediator (due to the light excitation of N–Ti–O) to promote the electron transfer between Au and TiO₂ induced by LSPR of Au nanoparticles under visible light irradiation. This work maybe provides an accessible way to the coupled of MOFs with semiconductor for CO oxidation.

Acknowledgments

This work was financially supported by the National Natural Science Foundation of China (no. 21273037), the National Basic Research Program of China (973 Program, no. 2014CB239303), the National Key Technologies R & D Program of China (no. 2014BAC13B03) and the Science & Technology Plan Project of Fujian Province (no.2014Y2003).

Appendix A. Supplementary data

Supplementary data associated with this article can be found, in the online version, at <http://dx.doi.org/10.1016/j.apcatb.2017.10.027>.

References

- [1] Y. Hartadi, R.J. Behm, D. Widmann, Methanol formation by CO_2 hydrogenation on Au/ZnO catalysts – effect of total pressure and influence of CO on the reaction characteristics, *Catalysts* 6 (2) (2016) 1–14.
- [2] G. Avgouropoulos, T. Ioannides, C. Papadopoulou, J. Batista, S. Hocevar, H. Matralis, A comparative study of $\text{Pt}/\gamma\text{-Al}_2\text{O}_3$, $\text{Au}/\alpha\text{-Fe}_2\text{O}_3$ and $\text{CuO}-\text{CeO}_2$ catalysts for the selective oxidation of carbon monoxide in excess hydrogen, *Catal. Today* 75 (2002) 157–167.
- [3] M. Haruta, Novel catalysis of gold deposited on metal oxides, *Catal. Surv. Asia* 1 (1997) 61–73.
- [4] D. Widmann, A. Krautsieder, P. Walter, A. Brückner, R. Behm Jr., How temperature affects the mechanism of CO oxidation on Au/TiO_2 : a combined EPR and TAP reactor study of the reactive removal of TiO_2 surface lattice oxygen in Au/TiO_2 by CO , *ACS Catal.* 6 (2016) 5005–5011.
- [5] A. Eliyas, P. Petrova, F. López-Tenllado, D. Tomova, A. Marinas, Experimental arrangements for determining the photocatalytic activity of Au/TiO_2 in air and wastewater purification, *Bulg. Chem. Commun.* 47 (2015) 978–984.
- [6] S. Tsubota, D. Cunningham, Y. Bando, M. Haruta, CO oxidation over gold supported on TiO_2 , *Stud. Surf. Sci. Catal.* 91 (1995) 227–235.
- [7] Z. Zhu, J.-L. Chang, R.-J. Wu, Fast ozone detection by using a core-shell Au/TiO_2 sensor at room temperature, *Sens. Actuators B: Chem.* 214 (2015) 56–62.
- [8] R. Zanella, S. Giorgio, C.-H. Shin, C.R. Henry, C. Louis, Characterization and reactivity in CO oxidation of gold nanoparticles supported on TiO_2 prepared by deposition-precipitation with NaOH andreae, *J. Catal.* 222 (2004) 357–367.
- [9] H. Zhu, Z. Wu, D. Su, G.M. Veith, H. Lu, P. Zhang, S.-H. Chai, S. Dai, Constructing hierarchical interfaces: TiO_2 -supported ptFe-FeO(x) nanowires for room temperature CO oxidation, *J. Am. Chem. Soc.* 137 (2015) 10156–10159.
- [10] M. Okumura, Y. Kitagawa, M. Haruta, K. Yamaguchi, DFT studies of interaction between O_2 and Au clusters: the role of anionic surface Au atoms on Au clusters for catalyzed oxygenation, *Chem. Phys. Lett.* 346 (2001) 163–168.
- [11] G.J. Kim, D.W. Kwon, S.C. Hong, The effect of pt particle size and valence state on the performance of Pt/TiO_2 catalysts for CO oxidation at room temperature, *J. Phys. Chem. C* 120 (2016) 17996–18004.
- [12] D. Gu, J.-C. Tseng, C. Weidenthaler, H.-J. Bongard, B. Spliethoff, W. Schmidt, F. Soulaimani, B.M. Weckhuysen, F. Schith, Gold on different manganese oxides: ultra-low-temperature CO oxidation over colloidal gold supported on bulk- MnO_2 nanomaterials, *J. Am. Chem. Soc.* 138 (2016) 9572–9580.
- [13] K. Hayek, M. Fuchs, B. Kötzer, W. Reichel, G. Rupprechter, Studies of metal-support interactions with real and inverted model systems: reactions of CO and small hydrocarbons with hydrogen on noble metals in contact with oxides, *Top. Catal.* 13 (2000) 55–66.
- [14] J.F. Liu, R.R. Si, H.R. Zheng, Q. Geng, W.X. Dai, X. Chen, X.Z. Fu, The promoted oxidation of CO induced by the visible-light response of Au nanoparticles over Au/TiO_2 , *Catal. Commun.* 26 (2012) 136–139.
- [15] J.M. Zamaro, A.V. Boix, A. Martínez-Hernández, CO oxidation over Au supported on Mn-ZSM5 and Mn-MOR , *Catal. Commun.* 69 (2015) 212–216.
- [16] M. Chen, D. Goodman, The structure of catalytically active gold on titania, *Science* 306 (2004) 252–255.
- [17] H. Yin, H. Kim, J. Choi, A.C. Yip, Thermal stability of ZIF-8 under oxidative and inert environments: a practical perspective on using ZIF-8 as a catalyst support, *Chem. Eng. J.* 278 (2015) 293–300.
- [18] X. Zhang, G. Li, S. Yang, X. Song, Z. Sun, Nanoporous CuO ribbons modified by Au nanoparticles through chemical dealloying and calcination for CO oxidation, *Microporous Mesoporous Mater.* 226 (2016) 61–70.
- [19] M.M. Schubert, S. Hackenberg, A.C.V. Veen, M. Muhler, V. Plzak, R.J. Behm, CO oxidation over supported gold catalysts—*inert* and active support materials and their role for the oxygen supply during reaction, *J. Catal.* 197 (2001) 113–122.
- [20] K. Yang, J. Liu, R. Si, X. Chen, W. Dai, X. Fu, Comparative study of Au/TiO_2 and $\text{Au}/\text{Al}_2\text{O}_3$ for oxidizing CO in the presence of H_2 under visible light irradiation, *J. Catal.* 317 (2014) 229–239.
- [21] K. Yang, K. Huang, Z. He, X. Chen, X. Fu, W. Dai, Promoted effect of PANI as electron transfer promoter on CO oxidation over Au/TiO_2 , *Appl. Catal. B: Environ.* 158 (2014) 250–257.
- [22] K. Yang, Y. Li, K. Huang, X. Chen, X. Fu, W. Dai, Promoted effect of PANI on the preferential oxidation of CO in the presence of H_2 over Au/TiO_2 under visible light irradiation, *Int. J. Hydrogen Energy* 39 (2014) 18312–18325.
- [23] K. Yang, K. Huang, L. Lin, X. Chen, W. Dai, X. Fu, Superior preferential oxidation of carbon monoxide in hydrogen-rich stream under visible light irradiation over gold loaded hedgehog-shaped titanium dioxide nanospheres: identification of copper oxide decoration as an efficient promoter, *J. Power Sources* 284 (2015) 194–205.
- [24] R. Banerjee, A. Phan, B. Wang, C. Knobler, H. Furukawa, M. O'Keeffe, O.M. Yaghi, High-throughput synthesis of zeolitic imidazolate frameworks and application to CO_2 capture, *Science* 319 (2008) 939–943.
- [25] B. Gole, U. Sanyal, R. Banerjee, P.S. Mukherjee, High loading of Pd nanoparticles by interior functionalization of MOFs for heterogeneous catalysis, *Inorg. Chem.* 55 (2016) 2345–2354.
- [26] H. Wu, W. Zhou, T. Yildirim, Hydrogen storage in a prototypical zeolitic imidazolate framework-8, *J. Am. Chem. Soc.* 129 (2007) 5314–5315.
- [27] A. Polyzoidis, T. Altenburg, M. Schwarzer, S. Loebbecke, S. Kaskel, Continuous microreactor synthesis of ZIF-8 with high space-time-yield and tunable particle size, *Chem. Eng. J.* 283 (2016) 971–977.
- [28] N. Dimitratos, A. Villa, D. Wang, F. Porta, D. Su, L. Prati, Pd and Pt catalysts modified by alloying with Au in the selective oxidation of alcohols, *J. Catal.* 244 (2006) 113–121.
- [29] N.L. Rosi, J. Eckert, M. Eddaoudi, D.T. Vodak, J. Kim, M. O'Keeffe, O.M. Yaghi, Hydrogen storage in microporous metal-organic frameworks, *Science* 300 (2003) 1127–1129.
- [30] M. Sadakiyo, S. Yoshimaru, H. Kasai, K. Kato, M. Takata, M. Yamauchi, A new approach for the facile preparation of metal-organic framework composites directly contacting with metal nanoparticles through arc plasma deposition, *Chem. Commun.* 52 (2016) 8385–8388.
- [31] L. Pan, B. Parker, X. Huang, D.H. Olson, J. Lee, J. Li, $\text{Zn}(\text{tbip})$ ($\text{H}_2\text{tbip} = 5$ -tert-butyl isophthalic acid): a highly stable guest-free microporous metal organic framework with unique gas separation capability, *J. Am. Chem. Soc.* 128 (2006) 4180–4181.
- [32] T.T. Isimjan, H. Kazemian, S. Rohani, A.K. Ray, Photocatalytic activities of $\text{Pt}/\text{ZIF-8}$ loaded highly ordered TiO_2 nanotubes, *J. Mater. Chem. B* 20 (2010) 10241–10245.
- [33] H. Wang, X. Yuan, Y. Wu, G. Zeng, H. Dong, X. Chen, L. Leng, Z. Wu, L. Peng, In situ synthesis of $\text{In}_2\text{S}_3@\text{MIL-125}(\text{Ti})$ core-shell microparticle for the removal of tetracycline from wastewater by integrated adsorption and visible-light-driven photocatalysis, *Appl. Catal. B: Environ.* 186 (2016) 19–29.
- [34] X. Yuan, H. Wang, Y. Wu, G. Zeng, X. Chen, L. Leng, Z. Wu, H. Li, One-pot self-assembly and photoreduction synthesis of silver nanoparticle-decorated reduced graphene oxide/MIL-125(Ti) photocatalyst with improved visible light photocatalytic activity, *Appl. Organomet. Chem.* 30 (2016) 289–296.
- [35] Z. Wu, X. Yuan, J. Zhang, H. Wang, L. Jiang, G. Zeng, Photocatalytic decontamination of wastewater containing organic dyes by metal-organic frameworks and their derivatives, *ChemCatChem* 9 (2017) 41–64.
- [36] M. Wen, Y. Cui, Y. Kuwahara, K. Mori, H. Yamashita, Non-noble-metal nanoparticle supported on metal-organic framework as an efficient and durable catalyst for promoting H_2 production from ammonia borne under visible light irradiation, *ACS Appl. Mater. Interfaces* 8 (2016) 21278–21284.
- [37] M. Wen, K. Mori, Y. Kuwahara, T. An, H. Yamashita, Design and architecture of metal organic frameworks for visible light enhanced hydrogen production, *Appl. Catal. B: Environ.* 218 (2017) 555–569.
- [38] C. Guo, M. Ge, L. Liu, G. Gao, Y. Feng, Y. Wang, Directed synthesis of mesoporous TiO_2 microspheres: catalysts and their photocatalysis for bisphenol A degradation, *Environ. Sci. Technol.* 44 (2010) 419–425.
- [39] G. Lu, S. Li, Z. Guo, O.K. Farha, B.G. Hauser, X. Qi, Y. Wang, X. Wang, S. Han, X. Liu, Imparting functionality to a metal-organic framework material by controlled nanoparticle encapsulation, *Nat. Chem.* 4 (2012) 310–316.
- [40] M. Du, J. Huang, X. Jing, D. Sun, Q. Li, Microorganism-mediated, CTAC-directed synthesis of SERS-sensitive Au nanohorns with three-dimensional nanostructures by *Escherichia coli* cells, *J. Chem. Technol. Biotechnol.* 4 (2015) 678–685.
- [41] X.Q. Deng, B. Zhu, X.S. Li, J.L. Liu, X. Zhu, A.M. Zhu, Visible-light photocatalytic oxidation of CO over plasmonic Au/TiO_2 : unusual features of oxygen plasma activation, *Appl. Catal. B: Environ.* 188 (2016) 48–55.
- [42] M. Wen, K. Mori, Y. Kuwahara, H. Yamashita, Plasmonic Au/Pd nanoparticles supported on a basic metal-organic framework: synergic boosting of H_2 production from formic acid, *ACS Energy Lett.* 2 (2017) 1–7.
- [43] Q. Sun, Y. Sun, T. Zhang, G. Chen, F. Zhang, D. Liu, W. Cai, Y. Li, X. Yang, C. Li, Complete Au/ZnO core-shell nanoparticles with enhanced plasmonic absorption enabling significantly improved photocatalysis, *Nanoscale* 8 (2016) 10774–10782.
- [44] J. Lee, E.V. Shevchenko, D.V. Talapin, Au-PbS core-shell nanocrystals: plasmonic absorption enhancement and electrical doping via intra-particle charge transfer, *J. Am. Chem. Soc.* 130 (2008) 9673–9675.
- [45] J.A. Singh, S.H. Overbury, N.J. Dudney, M. Li, G.M. Veith, Gold nanoparticles supported on carbon nitride: influence of surface hydroxyls on low temperature carbon monoxide oxidation, *ACS Catal.* 2 (2012) 1138–1146.
- [46] J. Zhu, S.A.C. Carabineiro, D. Shan, J.L. Faria, Y. Zhu, J.L. Figueiredo, Oxygen activation sites in gold and iron catalysts supported on carbon nitride and activated carbon, *J. Catal.* 274 (2010) 207–214.
- [47] D. Briggs, *Handbook of X-ray and Ultraviolet Photoelectron Spectroscopy*, Heyden, 1977.
- [48] R. Rajagopalan, J.O. Iroh, Characterization of polyaniline–polypyrrole composite coatings on low carbon steel: a XPS and infrared spectroscopy study, *Appl. Surf. Sci.* 218 (2003) 58–69.
- [49] I. Miloš, H.H. Strehblow, B. Navinšek, M. Metikoš-Huković, Electrochemical and thermal oxidation of TiN coatings studied by XPS, *Surf. Interface Anal.* 23 (1995) 529–539.
- [50] X. Chen, C. Burda, Photoelectron spectroscopic investigation of nitrogen-doped titania nanoparticles, *J. Phys. Chem. B* 108 (2004) 15446–15449.
- [51] D. Kim, S. Fujimoto, P. Schmuki, H. Tsuchiya, Nitrogen doped anodic TiO_2 nanotubes grown from nitrogen-containing Ti alloys, *Electrochim. Commun.* 10 (2008) 910–913.
- [52] J. Liu, J. He, L. Wang, R. Li, P. Chen, X. Rao, L. Deng, L. Rong, J. Lei, NiO-PTA supported on ZIF-8 as a highly effective catalyst for hydrocracking of *Jatropha* oil, *Sci. Rep.* 6 (2016) 23667.
- [53] A. Ghicov, J.M. Macak, H. Tsuchiya, J. Kunze, V. Haeublein, S. Kleber, P. Schmuki, TiO_2 nanotube layers: dose effects during nitrogen doping by ion implantation, *Chem. Phys. Lett.* 419 (2006) 426–429.
- [54] P. Ferstl, S. Mehl, M.A. Arman, M. Schuler, Adsorption and activation of CO on $\text{Co}_3\text{O}_4(111)$ thin films, *J. Phys. Chem. C* 119 (2015) 16688–16699.
- [55] Q. Yao, C. Wang, H. Wang, H. Yan, J. Lu, Revisiting the Au particle size effect on TiO_2 -coated Au/TiO_2 catalysts in CO oxidation reaction, *J. Phys. Chem. C* 120 (2016) 9174–9183.
- [56] A. Palazov, C. Chang, R. Kokes, The infrared spectrum of carbon monoxide on reduced and oxidized palladium, *J. Catal.* 36 (1975) 338–350.
- [57] R. Si, J. Liu, K. Yang, X. Chen, W. Dai, X. Fu, Temperature-programmed surface

reaction study of CO oxidation over Au/TiO₂ at low temperature: an insight into nature of the reaction process, *J. Catal.* 311 (2014) 71–79.

[58] J.D. Grunwaldt, M. Maciejewski, O.S. Becker, P. Fabrizioli, A. Baiker, Comparative study of Au/TiO₂ and Au/ZrO₂ catalysts for low-temperature CO oxidation, *J. Catal.* 186 (1999) 458–469.

[59] T. Fujitanil, I. Nakamura, Mechanism and active sites of the oxidation of CO over Au/TiO₂, *Angew. Chem. Int. Ed.* 2 (2011) 10144–10147.

[60] D. Widmann, R.J. Behm, Activation of molecular oxygen and the nature of the active oxygen species for CO oxidation on oxide supported Au catalysts, *Acc. Chem. Res.* 47 (2014) 740–749.

[61] M. Okumura, J.M. Coronado, J. Soria, M. Haruta, J.C. Conesa, EPR study of CO and O₂ interaction with supported Au catalysts, *J. Catal.* 203 (2001) 168–174.

[62] J. Panpranot, K. Kontapakdee, P. Praserttham, Effect of TiO₂ crystalline phase composition on the physicochemical and catalytic properties of Pd/TiO₂ in selective acetylene hydrogenation, *J. Phys. Chem. B* 110 (2006) 8019–8024.

[63] K. Yang, C. Meng, L. Lin, X. Peng, X. Chen, X. Wang, W. Dai, X. Fu, A hetero-structured TiO₂-C₃N₄ support for gold catalysts: a superior preferential oxidation of CO in the presence of H₂ under visible light irradiation or not, *Catal. Sci. Technol.* 6 (2016) 829–839.